Journal of Molecular Structure 1294 (2023) 136564

Contents lists available at ScienceDirect

Journal of Molecular Structure

journal homepage: www.elsevier.com/locate/molstr

Moderate DNA and high SARS-CoV-2 spike protein affinity of oxidovanadium(IV) complexes of 2-furoic acid hydrazones: In silico and in vitro approach

Adnan Zahirović [a,*], Burak Tüzün [b], Selma Hadžalić [a], Irnesa Osmanković [a], Sunčica Roca [c], Sabina Begić [a], Muhamed Fočak [d]

[a] Laboratory for Inorganic and Bioinorganic Chemistry, Department of Chemistry, Faculty of Science, University of Sarajevo, Zmaja od Bosne 35, 71000 Sarajevo, Bosnia and Herzegovina
[b] Plant and Animal Production Department, Technical Sciences Vocational School of Sivas, Sivas Cumhuriyet University, Sivas, Turkey
[c] Ruđer Bošković Institute, Zagreb, Croatia
[d] Department of Biology, Faculty of Science, University of Sarajevo, Sarajevo, Bosnia and Herzegovina

ARTICLE INFO

Keywords:
Vanadium(IV) hydrazone complexes
Salicylaldehyde
DNA
SARS-CoV-2
Molecular docking
Spike protein

ABSTRACT

The interaction of five neutral heteroleptic octahedral paramagnetic mononuclear oxidovanadium(IV) complexes of general composition [$V^{IV}O$(bpy)L], where L is a dianionic tridentate ONO-donor hydrazone ligand derived from 2-furoic acid hydrazide and salicylaldehyde and its 5-substituted derivatives with spike protein SARS-CoV-2 was investigated in silico and in vitro. Molecular docking indicates that the complexes have high affinity for SARS-CoV-2 spike protein binding, and that the complex with a nitro substituent on the salicylaldehyde component of the hydrazone ligand has the highest binding potential. The interaction of this complex was examined by spectrofluorimetry utilizing spectrofluorimetric titration, thermodynamic measurements and FRET analysis. The results suggest van der Walls forces and hydrogen bonding as the dominant modes of interaction of the complex with the SARS-CoV-2 spike protein, which is in agreement with theoretical predictions. Molecular docking was further employed to investigate the interaction of vanadium complexes with SARS-CoV-2 omicron variant (BA.1) RBD with human ACE2 protein. The interaction of the complex with CT DNA was investigated using electron spectroscopy and thermodynamic considerations. The complexes showed a moderate affinity for DNA as groove binders. The groove binding was confirmed by molecular docking with B-DNA. Also, druglikness properties of complexes were assessed by SwissADME. The strong antioxidant activity of the complexes, comparable to ascorbic acid, was evaluated by the DPPH method. This is the first experimental research that supports the thesis of molecular docking that vanadium compounds could be druggable against SARS-CoV-2 virus proteins.

1. Introduction

Living the last four years in the era of COVID-19 brightly shows that modern scientific community still cannot respond quickly and efficiently to the emergence of new diseases. Therefore, the design and development of new drugs, based on the well-defined principles of synthesis –structure – activity relationship, is essential in the field of drug discovery which should provide the accumulation of knowledge for rational postulation of the basic principles that determine the activity of drugs.

The outbreak of novel respiratory disease by the end of 2019 in Wuhan, China, shortly evolved into a pandemic COVID-19 caused by an easily-spared severe acute respiratory syndrome coronavirus 2 (SARS-CoV-2). Although the WHO has declared the end of the pandemic many unresolved questions concerning evolution and treatment of COVID-19 are still open. The absence of any prevention and treatment for this novel highly contagious respiratory disease practically paralyzed the modern world until the first vaccines were developed. Although vaccines are available today, their widespread use is limited by transportation, storage and administration problems along with the absence of mass-vaccination and concerns addressed by the anti-vaccination community [1,2]. Also, the effectiveness of vaccines in preventing the

* Corresponding author.
E-mail address: adnan.zahirovic@pmf.unsa.ba (A. Zahirović).

https://doi.org/10.1016/j.molstruc.2023.136564
Received 7 June 2023; Received in revised form 31 August 2023; Accepted 1 September 2023
Available online 2 September 2023

disease is frequently questioned due to the high mutation ability of SARS-CoV-2 whose variants easily bypass the immune response of the vaccinated person causing an infection [3]. Thus, increased attention is devoted to the development of antiviral drugs that can prevent virus replication by aiming the less specific targets than vaccines. Several known drugs, such as favipiravir, have been investigated for their antiviral potential in COVID-19 treatment [4].

Recently, several research groups have employed molecular docking approach to postulate that vanadium complexes could be druggable against the SARS-CoV-2 main protease, the SARS-CoV-2 RNA-dependent polymerase, and the N-terminal RNA binding domain of the SARS-CoV-2 nucleocapsid phosphoprotein [5,6]. Inspired by their findings and the fact that both, hydrazones [7,8] and vanadium compounds [9–11], possess antiviral potential and strongly encouraged by the antiviral properties of salicyl hydrazones [12] and molecules with furan-containing moieties [13,14], joined with the vivid ability of vanadium complexes to interact with proteins [5], along with empirically established fact that coordination to a metal center results with an increased biological activity of the complexes compared to native ligands, we investigated five novel vanadium(IV) complexes with 2-furoic acid hydrazones of salicylaldehyde and its 5-substituted derivatives, recently prepared in our laboratory [15], as potential SARS-CoV-2 spike protein binders.

The spike protein, along with the membrane glycoprotein (M), an envelope protein (E), and the nucleocapsid protein (N), is one of the four structural proteins of the SARS-CoV-2 virus and is responsible for binding to the ACE2 receptor, allowing the virus to enter the host cell [16]. Considering this crucial role of the spike protein in the life cycle of virus, binding of vanadium complexes to spike protein would potentially preclude molecular recognition among the ACE2 receptor and the spike protein, thus preventing the virus entrance to the cell and consequently its replication (Fig. 1). Moreover, the spike protein is the primary target of neutralizing antibodies [17] and thus imposes itself as an important molecular target for potential antiviral drugs.

Despite the reasonable potential of vanadium compounds for spike protein binding, their therapeutic potential could be limited by their particularly high affinity for transport proteins, especially albumins. Generally, a large binding constant of drugs with proteins leads to strong, most often irreversible binding, which sometimes results in drugs being inactivated before reaching their molecular target [18–21]. Certainly, the exceptions are compounds whose intentional binding to a protein increases their bioactivity. The vanadium complexes having a moderate affinity toward BSA, would give good candidates for testing their spike protein binding affinity. In this context, five novel heteroleptic vanadium(IV) complexes of salicylaldehyde-based 2-furoic acid hydrazones prepared in our laboratory, which are moderate BSA binders [15], are good potential candidates for spike protein SARS-CoV-2 binding.

Here, we report the interaction of vanadium(IV) complexes of salicylaldehyde-based 2-furoic acid hydrazones featuring bipyridine coligand with SARS-CoV-2 spike protein (PDB ID: 7DDN) and SARS-CoV-2 omicron variant (BA.1) RBD with human ACE2 protein (PDB ID: 7U0N) in silico, along with the in vitro SARS-CoV-2 spike protein – complex interaction, as a pioneering work in this field. Moreover, we investigated the interaction of complexes with CT DNA in vitro and with B-DNA in silico (PDB ID: 1BNA) and tested their antioxidant activity and druglikness properties using SwissADME tools.

2. Experimental

2.1. Chemicals

All chemicals used for synthese, and interaction with SARS-CoV-2 spike protein and CT DNA were of analytical grade unless otherwise stated. Recombinant 2019-nCoV Spike S1 Protein with His tag (S glycoprotein Subunit 1, S1 protein) expressed in HEK 293 cells was obtained as lyophilized powder (>95% HPLC, 75.8 kDa) from Sigma Aldrich. Highly polymerized deoxyribonucleic acid sodium salt from calf thymus (CT DNA), Type I, fibers ($A_{260}/A_{280} > 1.8$) was acquired also from Sigma Aldrich. Vanadium complexes of salicylaldehyde based 2-furoic acid hydrazones were prepared by a reported procedure [15] and their identity and purity confirmed through elemental analysis and infrared spectra.

2.2. Physical measurements

The interaction of complexes with SARS-CoV-2 spike protein were investigated by spectrofluorimetry. Spike protein (S) (100 μg) was dissolved in 2.000 mL of 10 mM phosphate buffer and stirred for two hours at ambient conditions. An aliquot of solution (1000 μL) was diluted to 10.00 mL with phosphate buffer and concentration of protein was determined from electronic spectrum ($\lambda_{max} = 280$ nm) using an extinction coefficient of 91 775 M^{-1} cm^{-1} calculated from amino acid sequence given in Supplement using a ProtParam [22]. Electronic spectra were recorded using a Perkin Elmer BioLambda 35 in the range 200–1100 nm. The spectrofluorimetric titration was carried out by successive additions of 10-μL portion of complex (5.00×10^{-4} M, MeOH) to spike protein (2.000 mL, 2.30×10^{-7} M) with equilibrium

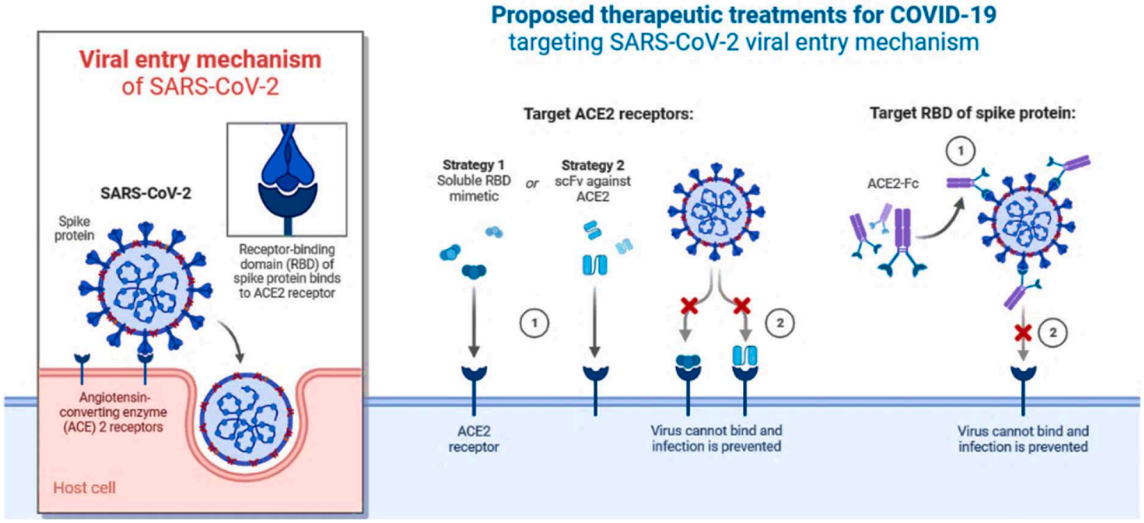

Fig. 1. SARS-CoV-2 viral entry mechanism and proposed therapeutic treatments targeting viral entry mechanism.

time $t = 5$ min. Emission spectra were recorded in 290–440 nm using a 275 nm as excitation wavelength. Measurements were done on a Shimadzu RF 6000 at three temperatures (296, 301, 310 K). The three-dimensional emission spectra of spike protein were recorded in 300–500 nm region using a 5 nm increments in excitation wavelength in 200–285 nm region.

The interactions of DNA and corresponding vanadium(IV) complexes were carried out in 10 mM Tris–HCl buffer pH 7.42 using a method of spectroscopic titration. The stock solution of CT DNA was prepared in 10 mM Tris–HCl buffer pH 7.42 by the continuous stirring of CT DNA for 24 h to assure proper hydration and to obtain millimolar concentration of the stock solution. The concentration and purity of CT DNA were determined based on the extinction coefficient of 6600 M^{-1} cm^{-1} at 260 nm (7.20 mM, $A_{260}/A_{280} = 1.83$, $A_{230}/A_{260} = 0.39$). Stock solutions of complexes (1 mM) were prepared in MeOH. Working solutions of compounds (5×10^{-5} M) were always freshly prepared by diluting aliquot (100 μL) of MeOH stock solution of compounds by Tris–HCl buffer up to a volume of 2000 μL. Thus obtained solutions were used for spectroscopic titration of the compound with DNA by successive addition of 10-microliter amounts of CT DNA stock solution and recording the electronic spectra in 250–500 nm range. The equilibration time after each addition of DNA was 5 min.

The antioxidant activity of the complexes was determined by the DPPH radical scavenging method [23].

2.3. Molecular docking calculations

Quantum chemical calculations for vanadium complexes were done as reported earlier [15]. The interaction of complexes with SARS-CoV-2 spike protein was investigated using the HEX software program [24] and PLIP (Protein–Ligand Interaction Profiler) analysis was employed to get deeper insight into these interactions [25]. Hex uses a simple clustering algorithm to group spatially similar docking orientations. At HEX 8.0.0, the protein and molecule files were examined [25]. For docking, the following variables are used: Correlation type shape only, 3D FFT mode, 0.6-dimensional grid, 180-degree receptor and ligand ranges, 360-degree twist range, and 40-degree distance range. The crystal structure of SARS-CoV-2 spike protein as a target molecule was reported by Zhang et al. [26] and accessed through PDB code 7DDN. The crystal structure of SARS-CoV-2 omicron variant (BA.1) RBD with human ACE2 protein is available through PDB code 7U0N and was recently reported by Geng et al. [27]. The interaction of complexes with synthetic DNA dodecamer d(CpGpCpGpApApTpTpCpGpCpG) reported by Drew et al. [28] (PDB code: 1BNA) was also investigated.

3. Results and discussion

3.1. Oxidovanadium(IV) complexes

During the last two years several research groups postulated that vanadium compounds, including its coordination complexes [5,6] and polyoxovanadates [29], could be druggable against SARS-CoV-2 virus targeting different proteins including spike protein responsible for viral entry to host cells. As pointed out in Introduction, vanadium(IV) complexes are good candidates for antiviral drug discovery as their well-defined and controllable structure-dependent redox properties and ligand substitutions, coupled with empirically established antiviral activity and further joined with vivid ability to bind proteins as main biomolecular targets of viruses. The oxidovanadium(IV) complexes featuring salicylaldehyde based 2-furoic acid hydrazones and bipyridine coligand were recently published by our research group [15] and their structural formula is shown in Fig. 2 and abbreviated as (**1**)–(**5**).

Complexes are neutral heteroleptic mononuclear species having vanadium(IV) embedded in octahedral coordination by bipyridine nitrogen and tridentate ONO donor hydrazone ligand and one terminal oxygen. The structural difference among complexes is substituent in

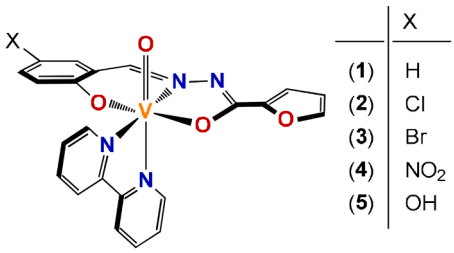

Fig. 2. Structural formula of vanadium(IV) hydrazone complexes (**1**)–(**5**).

position 5 on salicylaldehyde part of hydrazone ligand which affects electron density on hydrazone ligand and consequently reactivity of molecular specie to different biological targets. Previously we showed that complexes (**1**)–(**5**) have only moderate affinity to BSA compared to a large number of vanadium complexes that are strong BSA binders. The moderate affinity to BSA (in vitro and in vivo), and reversibility of this binding, qualify vanadium complexes (**1**)–(**5**) as promising candidates for further biological testing due to their potential to bind divergent biological targets as they are not strongly deactivated by albumin binding.

3.2. SARS-CoV-2 spike protein spectral features

The spike protein of SARS-CoV-2 is a glycoprotein and the largest among the four main structural proteins of the virus, along with the membrane glycoprotein (M), an envelope protein (E), and the nucleocapsid protein (N) [30]. The receptor for spike protein is angiotensin-converting enzyme 2 (ACE2) and this interaction facilitates virus entry to host cell [16]. Recombinant 2019-nCoV Spike S1 Protein with His tag (S glycoprotein Subunit 1, S1 protein) produced by expression in HEK 293 cells was obtained as lyophilized powder (>95% HPLC, 75.8 kDa) and used for experimental measurements. The protein was reconstituted in phosphate buffer and used no longer than 2 day for experimental measurements.

The electron absorption spectra of spike protein is shown in Fig. 3a and shows typical protein absorption band near 280 nm. The extinction coefficient of spike protein with His tag was determined by ProtParam [22] based on the amino acid sequence given in Supplement ($\varepsilon = 91\,775$ M^{-1} cm^{-1}). The fluorescence of spike protein is anticipated as it comprises seven tryptophan, thirty-five tyrosine and forty-seven phenylalanine residues which are predominantly responsible for protein emission spectra. When excited at 275 nm spike protein shows two emission bands near 305 and 340 nm. The emission intensity of these bands is temperature dependent (Fig. 3b) indicating protein conformational change with temperature increase.

3.3. In silico interaction with SARS-CoV-2 proteins

Quantum chemical calculations on electron densities and orbital energies only partially described the anticipated biological activity of metal complexes and molecular docking is regularly employed for gathering the insight into the reactivity of metal complexes to predefined biomolecular targets thus providing valuable information on structure–activity relationship. The interactions of vanadium complexes (**1**)–(**5**) with SARS-CoV-2 spike protein were investigated using HEX software to find the best candidate for experimental measurements. The crystal structure of SARS-CoV-2 spike protein was reported by Zhang et al. [26] and accessed through PDB code 7DDN. The crystal structure SARS-CoV-2 omicron variant (BA.1) RBD with human ACE2 protein is available through PDB code 7U0N and was recently reported by Geng et al. [27]. The total energy values for these interactions are given in Table 1.

The lowest total energy value for interaction with SARS-CoV-2 spike protein was obtained for complex (**4**) having vanadium(IV) coordinated

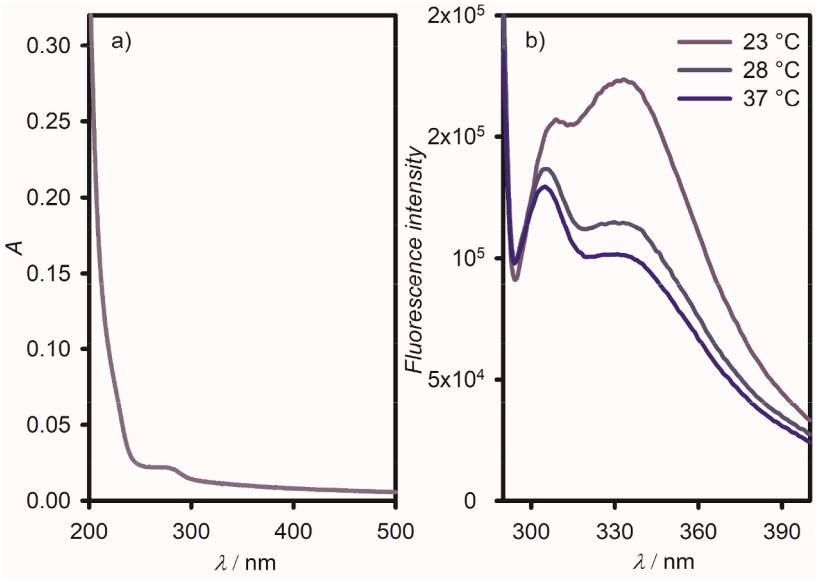

Fig. 3. Electron absorption (a) and emission (b) spectra of SARS-CoV-2 spike protein (2.30×10^{-7} M).

Table 1
The total energy values (kcal/mol) for the interaction of (**1**)–(**5**) with SARS-CoV-2 spike protein and SARS-CoV-2 RBD ACE2 protein.

	E_{total} with SARS-CoV-2 spike protein	E_{total} with SARS-CoV-2 RBD ACE2 protein
(**1**)	−223.05	−299.94
(**2**)	−233.35	−308.05
(**3**)	−231.71	−296.12
(**4**)	−266.89	−312.93
(**5**)	−232.66	−304.78

by 5-nitro-salicilydehyde 2-furoic acid hydrazone. Vanadium(IV) complexes (**2**), (**3**), and (**5**), featuring 5-chloro, 5-bromo, and 5-hydroxy substituent on salicylaldehyde part of hydrazone ligand, respectively, have close E_{total} values for interaction with SARS-CoV-2 spike protein, increasing in order chloro (**2**) < hydroxyl (**5**) < bromo (**3**). Complex (**1**) with unsubstituted salicylaldehyde 2-furoic acid hydrazone has the highest E_{total} value indicating its lowest potential to bind spike protein. Interestingly, complex (**4**) showed also the highest potential to bind with SARS-CoV-2 omicron variant (BA.1) RBD with human ACE2 protein and the binding energy increases in order (**4**) < (**2**) < (**5**) < (**1**) < (**3**).

Considering that hydrogen bonding, polar and hydrophobic interaction, along with π−π and halogen interactions between metal complexes and protein targets determines their biological activity [31,32], the interactions of vanadium complexes with the SARS-CoV-2 spike protein and SARS-CoV-2 omicron variant (BA.1) RBD with human ACE2 protein were analyzed by Protein-Ligand Interaction Profiler (PLIP). The visual representations of the obtained results and binding poses of complexes to SARS-CoV-2 spike protein are shown in Figs. 4 and 5. The predominant type of the interactions between vanadium complexes and spike protein is hydrophobic interactions, observed in all cases except for complex (**5**) (Table 3). On the other hand, complex (**5**), along with complex (**2**) shows hydrogen binding to spike protein (Table 4).

On the other hand, the hydrophobic interactions (Table 2), as well as hydrogen bonding (Table 3) are more pronounced in interaction of SARS-CoV-2 omicron variant (BA.1) RBD with human ACE2 protein and complex, compared to spike protein – complex interactions.

The hydrophobic interactions of vanadium complexes (**1**)–(**4**) with amino acid residues of SARS-CoV-2 spike protein involve mostly Leucine–981A [(**1**) and (**3**)] and Proline-986C [(**2**), (**3**) and (**4**)], while the additional interaction with Glutamic acid–748C residue was observed for complex (**3**). The hydrogen bonding of complex (**2**) with Asparagine–751C and complex (**5**) with Isoleucine–587C was observed. The hydrophobic interaction and hydrogen boding of complexes (**1**)–(**5**) with amino acid residues of SARS-CoV-2 spike protein are shown in Fig. 6. Halogen or π−π interactions were not observed in any case.

All five vanadium complexes, including complex (**5**) featuring hydroxyl substituent, showed hydrophobic interaction with SARS-CoV-2 omicron variant (BA.1) RBD with human ACE2 protein. In all cases interaction involve Glutamic acid. Hydrophobic interaction with Proline were observed for complexes (**3**) and (**5**). Additionally, complex (**5**) displays interactions with Glutamine, Isoleucine and Valine. Hydrogen bonding also plays an important role in vanadium complex interactions with SARS-CoV-2 RBD ACE2 protein and this type of bonding was not observed only for complex (**3**). Hydrogen boding with Lysine is anticipated for (**1**) and (**2**), while interactions with Threonine for (**4**) and Glutamine for (**5**) were observed.

3.4. *In vitro interaction with SARS-CoV-2 spike protein*

The molecular docking showed the highest affinity of complex (**4**) featuring nitro substituent on salicylaldehyde component of hydrazone ligand in oxidovanadium(IV) complexes and thus was selected for further measurements. The interaction of complex (**4**) with recombinant 2019-nCoV Spike S1 Protein with His tag was investigated by spectrofluorimetric titration. In presence of an increasing concentrations of complex pronounced fluorescence quenching for spike protein was observed (Fig. 7a). The decrease of emission intensity is linear and Stern–Volmer equation could be applied to determine Stern–Volmer binding constant (K_{SV}) as a slope from the plot I_0/I versus concentration of complex, where I_0 and I are the emission intensities in absence and presence of different concentrations of complex, respectively (Fig. 7b). The observed K_{SV} value of 10^5 M^{-1} order at 23 °C indicate strong interaction of complex (**4**) with spike protein (Table 4). As the temperature increases the decrease of K_{SV} value was observed indicating the decrease in complex – protein binding.

The binding constant (K_b) was calculated from linear plot of $\log[(I_0 - I)/I]$ vs. log[complex] using Eq. (1):

$$\log\frac{I_0 - I}{I} = \log K_b + n\ \log[\text{complex}] \quad (1)$$

where I_0 and I are emission intensities of protein in absence and presence of increasing concentrations of complex and n is the number of the

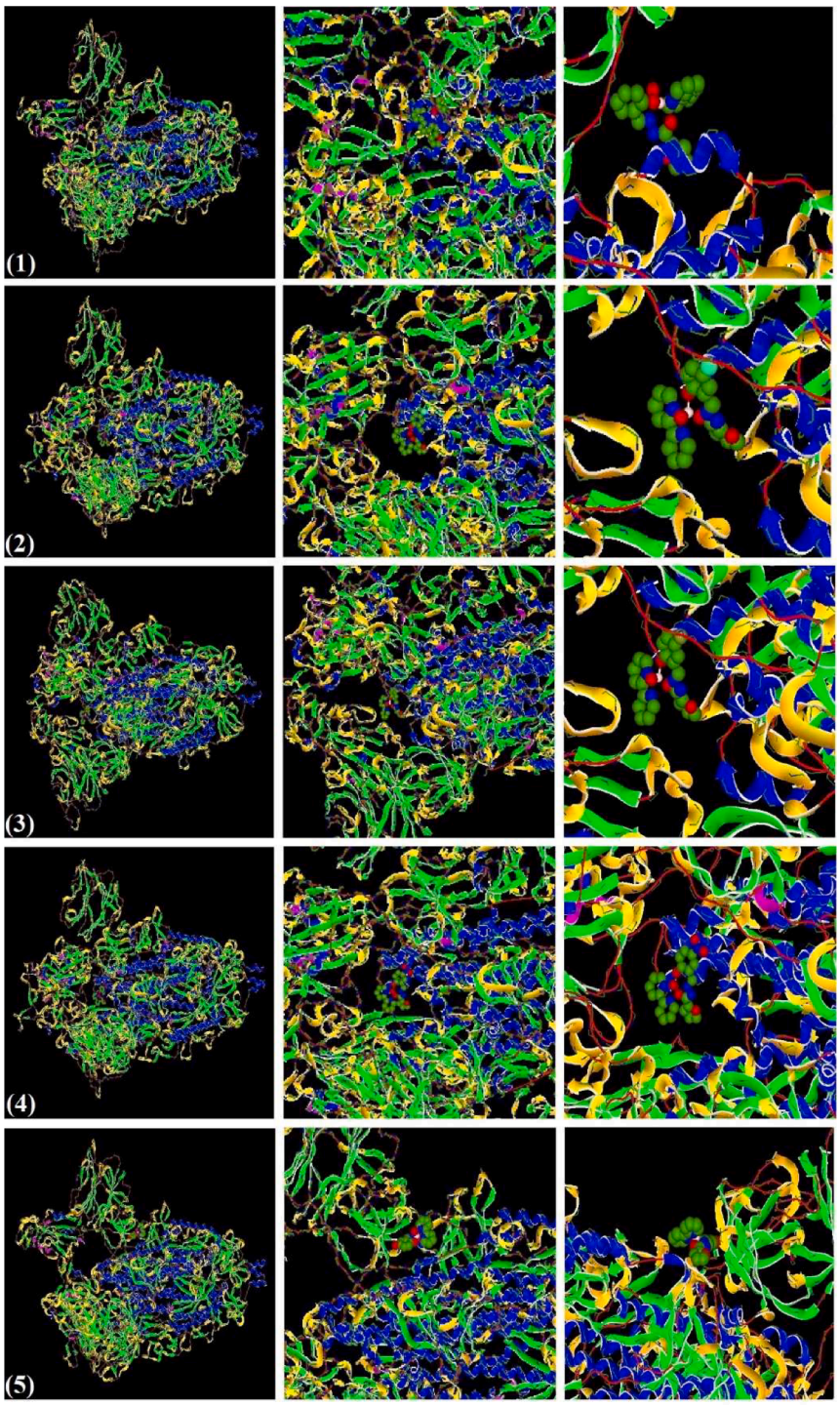

Fig. 4. Binding poses of (**1**)–(**5**) complexes to SARS-CoV-2 spike protein (left) and enlarged regions of binding (middle and right).

binding sites. The binding constant decreases with an increase of temperature and at 23 °C was found as 2.99×10^5 M^{-1} confirming strong interaction among spike protein and complex (**4**). Comparing the reactivity of the same complex to BSA K_b value was reported as 1.07×10^4 M^{-1} [15], making the binding constant of complex (**4**) to SARS-CoV-2 spike protein 30 times higher compared to the one reported for binding to albumin. The observed decrease of the K_b value (Table 4) with a temperature increase indicates that complex−protein adduct is more prone to dissociation at elevated temperatures. The number of the binding sites (n) of complex to spike protein is near 1 indicating the formations of 1:1 adduct. The quenching rate constant ($k_q > 1.01 \times 10^{13}$ M^{-1} s^{-1}) confirm static quenching mechanism since the maximal k_q value for dynamic quenching is 2×10^{10} M^{-1} s^{-1} [33].

The three-dimensional spectra of spike protein in absence and presence of complex (**4**) give deeper insight to emission changes of spike protein (Fig. 8). When excitation wavelength is varied in 200–285 nm range two emission regions arise. Emission of spike protein can be triggered by excitation at 210 nm and 275 nm. In both cases, emission band with maximum near 340 nm is observed (Fig. 8a). The strong fluorescence quenching of spike protein is found in presence of complex regardless on excitation wavelength used (Fig. 8b and c).

In absence of structural evidence thermodynamics provide valuable

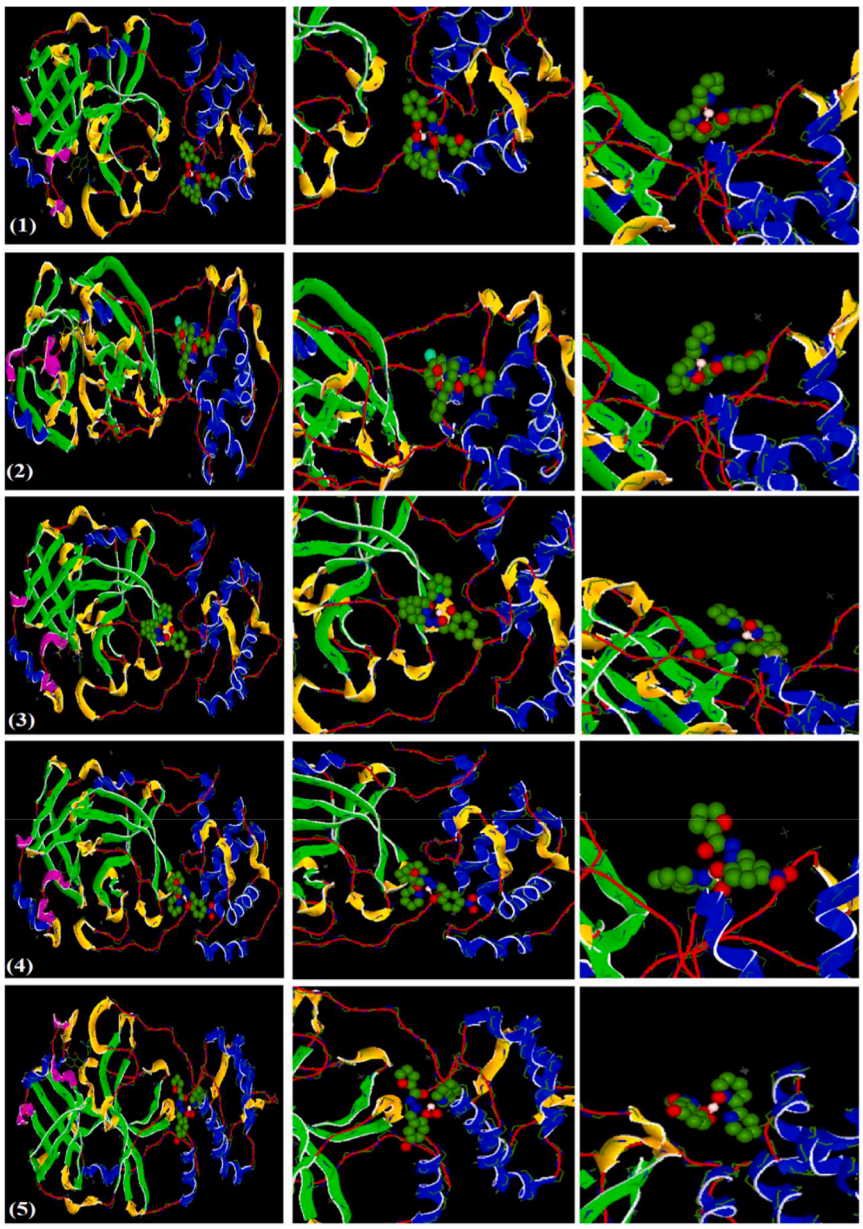

Fig. 5. Binding poses of (**1**)–(**5**) complexes to SARS-CoV-2 omicron variant (BA.1) RBD with human ACE2 protein (left) and enlarged regions of binding (middle and right).

tools for assessing the nature of the forces responsible for protein – complex binding. As the measurement for spike protein – complex interaction were conducted at tree temperatures thermodynamic data were obtained from van't Hoff plot (Fig. 9) using Eq. (2):

$$lnK = -\frac{\Delta H}{RT} + \frac{\Delta S}{R} \tag{2}$$

where R is gas constant. The entropy change (ΔS) and enthalpy change (ΔH) are graphically obtained from ln$K$b vs. $1/T$ graph. Considering that the temperature interval is narrow enthalpy change can be considered constant and temperature independent and Gibbs free energy (ΔG) can be calculated using Eq. (3):

$$\Delta G = \Delta H - T\Delta S \tag{3}$$

The negative value of ΔG (Table 4) confirms that the interaction of complex with spike protein is spontaneous in investigated temperature range. Nonetheless, ΔG is not indicative for type of the biding forces that dominate nature of protein – complex binding. The type of forces involved in interaction can be elucidated from ΔH and ΔS values since different types of forces that govern these interactions result in substantially different values of these thermodynamic functions. There are several potential scenarios for protein – complex interaction and these include electrostatic interaction, hydrophobic interactions, covalent binding and van der Waals and hydrogen bonding. The electrostatic interactions result with positive ΔS values and ΔH close to zero and can be excluded in case of spike protein – vanadium complex (**4**) interaction [34,35]. Also, the observed negative value of ΔH for the interaction also eliminates covalent binding since in the positive and large value of ΔH is expected ($\Delta H > 120$ kJ mol^{-1}) [36]. Hydrophobic interaction results in positive values of both, ΔH and ΔS [34,35] and thus cannot be postulated based on the experimental results, although it could not be a priori excluded as a hypothesis based on the structure of vanadium complex (**4**) having hydrophobic regions. The experimentally observed negative values of ΔH and ΔS are consistent with van der Walls forces and hydrogen bonding as the predominant type of the forces that govern the interaction of spike protein and complex (**4**), which is in excellent

Table 2
Hydrophobic Interactions of SARS-CoV-2 spike protein and SARS-CoV-2 omicron variant (BA.1) RBD with human ACE2 protein with vanadium complex (**1**)–(**5**).

Complex	Residue	AA	Distance	Ligand atom	Protein atom
SARS-CoV-2 spike protein					
(1)	981A	LEU	3.20	30,641	8604
(2)	986C	PRO	3.07	30,610	18,860
(3)	748C	GLU	3.92	30,628	16,816
	981C	LEU	3.96	30,634	18,809
	981C	LEU	3.80	30,633	18,807
	986C	PRO	2.61	30,610	18,860
(4)	986C	PRO	2.98	30,610	18,860
SARS-CoV-2 ACE2 protein					
(1)	290A	GLU	2.86	2926	2703
(2)	5A	LYS	2.61	2900	51
	136A	ILE	3.38	2934	1298
	289A	ASP	4.00	2926	2693
(3)	748C	GLU	3.92	30,628	16,816
	981C	LEU	3.96	30,634	18,809
	981C	LEU	3.80	30,633	18,807
	986C	PRO	2.61	30,610	18,860
	986C	PRO	2.98	30,610	18,860
(4)	197A	ASP	3.74	2902	1838
	239A	TYR	3.62	2926	2254
	290A	GLU	3.93	2909	2703
(5)	107A	GLN	3.83	2921	1033
	108A	PRO	3.91	2932	1045
	132A	PRO	3.64	2934	1259
	200A	ILE	3.41	2900	1867
	202A	VAL	2.76	2900	1884
	240A	GLU	3.02	2899	2264

accordance with the results of molecular docking (*vide supra*) [37]. This credits molecular docking as a powerful tool in a quest of new potential drug candidates capable of spike protein binding and encourage further testing of vanadium complexes as promising protein-selective anti--SARS-CoV-2 agents as postulated by molecular docking [5,6].

Forster's theory was further used to assess fluorescence resonance energy transfer and the distance between fluorophore and the complex at which the energy transfer occurs. The efficiency of the energy transfer can be calculated using Eq. (3) from fluorescence intensities of spike protein in the presence (I) and absence (I_0) of the complex (**4**) [38]:

$$E = 1 - \frac{I}{I_0} = \frac{R_0^6}{R_0^6 + r^6} \tag{3}$$

When the transfer efficiency is 50% the distance between the donor and acceptor (r) and critical distance (R_0) can be calculated using Eq. (4) after experimental determination of the overlapping integral value (J) [38]

$$R_0^6 = 8.8 \times 10^{-25} K^2 \Phi J N^{-4} \tag{4}$$

where $K^2 = 2/3$, $N = 1.33$ and $\varphi = 0.383$ are constants for spike protein [37]. The overlapping integral value is obtained from fluorescence intensity of the fluorescent donor ($F(\lambda)$) at the wavelength λ and the extinction coefficient ($\varepsilon(\lambda)$) using Eq. (5) [39]

$$J = \frac{\sum F(\lambda)\varepsilon(\lambda)\lambda^4 \Delta\lambda}{\sum F(\lambda)\Delta\lambda} \tag{5}$$

The overlap of emission spectrum of SARS-CoV-2 spike protein and absorption spectrum of oxidovanadium(IV) complex (**4**) is given in Fig. 10 and the overlapping integral value was determined as $J = 2.09 \times 10^{-14}$ cm^3 M^{-1}. The critical distance is $R_0 = 3.38$ nm, while the distance value $r = 3.03$ nm confirms that non-radiative energy transfer took a place, which is evident when r values lower than 8 nm are found [40]. The obtained values of r and R_0 are similar to those reported for energy transfer between tryptophan capped gold-aryl nanoparticles and SARS-CoV-2 spike protein [37].

3.5. Interaction with DNA

DNA is considered one of the primary intracellular targets of novel metal-based drugs. The antitumor activity of platinum-based drugs and the antibacterial activity of nucleic acid inhibitor antibiotics demonstrate that the interaction of drugs with DNA can be closely related to their mechanism of action [41]. The interactions of novel metal complexes with DNA are not only crucial from the aspect of designing new and promising drugs, they also play a major role in the discovery of probes for nucleic acids, DNA footprinting, and sequence-specific cleaving agents [42]. The interaction of vanadium complexes (**1**)–(**5**) with CT DNA was investigated by electron spectroscopy using the spectrophotometric titration approach.

The typical spectroscopic titration of (hydrazonato)oxidovanadium (IV) complex (**1**)–(**5**) with CT DNA reveals moderate hypochromism of LMCT bands of the complex in the presence of an increasing amount of DNA (Fig. 11; Figs. S1−S6). The binding constants (K_b) were graphically determined as described elsewhere [43] and their values are summarized in

Table 5. Different binding modes of vanadium complexes to DNA can be expected, ranging from electrostatic, over hydrophobic to intercalation and covalent binding. However, sterically closed and hydrolytically stable oxidovanadium(IV) complexes of salicylaldehyde 2-furoic acid hydrazones (**1**)–(**5**) meet the criteria for non-covalent interactions. The intercalation and hydrophobic groove binding are reasonably expected. The moderate values of the binding constants ranging from 1.76×10^3 M^{-1} to 1.38×10^4 M^{-1}, along with the absence of bathochromic shift of charge transfer bands excludes intercalation and nominate groove binding as the most likely type of interaction as later confirmed by thermodynamic measurements (*vide infra*).

The binding constant for oxidovanadium(IV) complexes (**1**)–(**5**) are substituent depended and range over a 10-order magnitude. The largest binding constant was found for complex (**2**) bearing chloro substituent at the salicylaldehyde part of the hydrazone ligand. The K_b values decrease in order Cl > Br > OH > NO_2 > H, indicating that the aldehyde part of hydrazone ligand in oxidovanadium(IV) complexes plays

Table 3
Hydrogen Bonds in SARS-CoV-2 spike protein and SARS-CoV-2 omicron variant (BA.1) RBD with human ACE2 protein interactions with vanadium complexes (**1**)–(**5**).

Complex	Residue	Amino acid	Distance H-A	Distance D-A	Donor angel	Protein donor	Side chain	Donor atom	Acceptor atom
SARS-CoV-2 spike protein									
(2)	751C	ASN	3.29	4.10	138.63	Yes	Yes	16,843 [Nam]	30,641 [O2]
(5)	587C	ILE	2.50	3.03	113.19	No	No	30,647 [O2]	15,673 [O2]
SARS-CoV-2 ACE2 protein									
(1)	137A	LYS	3.60	3.94	101.86	Yes	Yes	1311 [N3+]	2894 [O3]
(2)	287A	LEU	2.59	3.59	171.36	Yes	No	2670 [Nam]	2933 [O2]
	5A	LYS	2.91	3.56	120.63	Yes	Yes	53 [N3+]	2895 [O2]
	137A	LYS	1.18	2.10	147.07	Yes	No	1303 [Nam]	2933 [O2]
(4)	199A	THR	2.88	3.65	136.81	No	Yes	2894 [O3]	1857 [O3]
	199A	THR	3.06	3.55	113.80	Yes	Yes	1857 [O3]	2895 [O2]
(5)	110A	GLN	2.52	2.88	101.17	Yes	Yes	1061 [Nam]	2939 [O2]

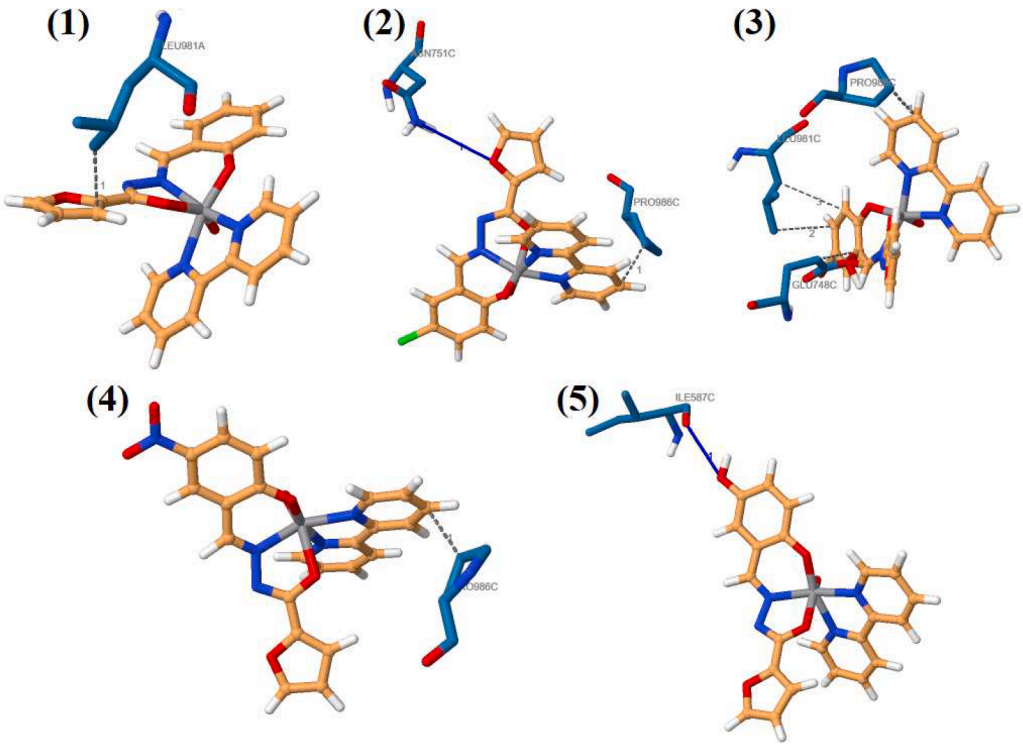

Fig. 6. The close-up view of interaction of (**1**)–(**5**) with SARS-CoV-2 spike protein.

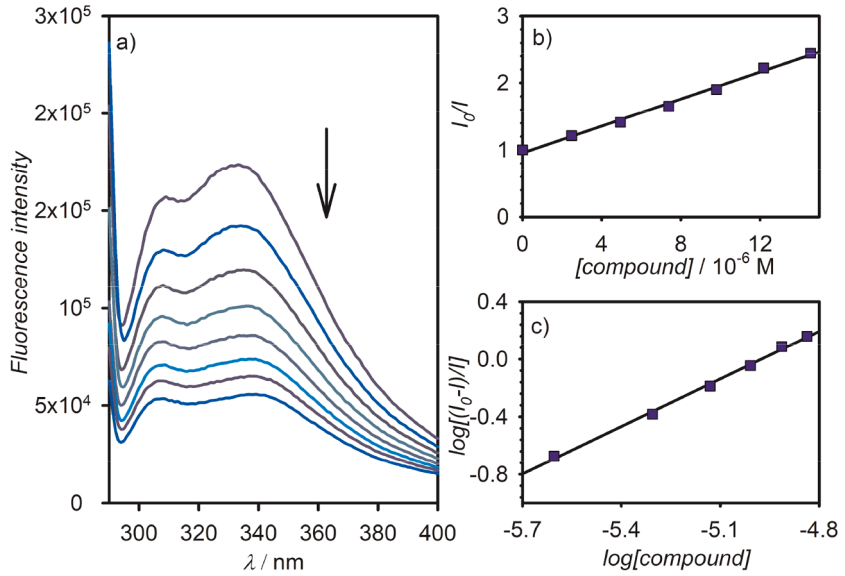

Fig. 7. Interaction of (**4**) with SARS-CoV-2 spike protein: (a) spectrofluorimetric titration of spike protein with complex; (b) graphical determination of Stern–Volmer constant; (c) graphical determination of binding constant.

Table 4
Thermodynamic data on interaction of complex (**4**) with SARS-CoV-2 spike protein.

t /°C	K_{SV} / 10^5 M^{-1}	k_q / 10^{12} M^{-1} s^{-1}	K_b / 10^5 M^{-1}	n	ΔH / kJ mol^{-1}	ΔS / J mol^{-1} K^{-1}	ΔG / kJ mol^{-1}
23	1.01	10.1	2.99	1.10	−100	−231	−31.5
28	0.49	4.93	2.46	1.15			−30.4
37	0.46	4.64	0.52	1.01			−28.3

important role in DNA – complex interactions.

The DNA binding constant values for complexes (**1**)–(**5**) are lower compared to binuclear vanadium(V) complexes featuring 2-hydroxybenzoylhydrazones of acetylacetone and benzoylacetone [44] and [$V^{IV}OL^2$] complexes, where L is 5-nitro-salicylaldehyde 2,4-dinitrophenylhydrazone [45]. Structurally similar [VO(phen)L] complex with 5-hydroxybenzaldehyde benzoylhydrazone is also a stronger DNA binder compared to (**1**)–(**5**) complexes with $K_b = 4.6 \times 10^5$ M^{-1} and binds DNA through intercalative mode [46]. Many vanadium(V) hydrazone complexes such as [$V^{V}O(L)(hq)$] complexes featuring 2-hydroxybenzoylhydrazones of 2-hydroxyacetophenone and its

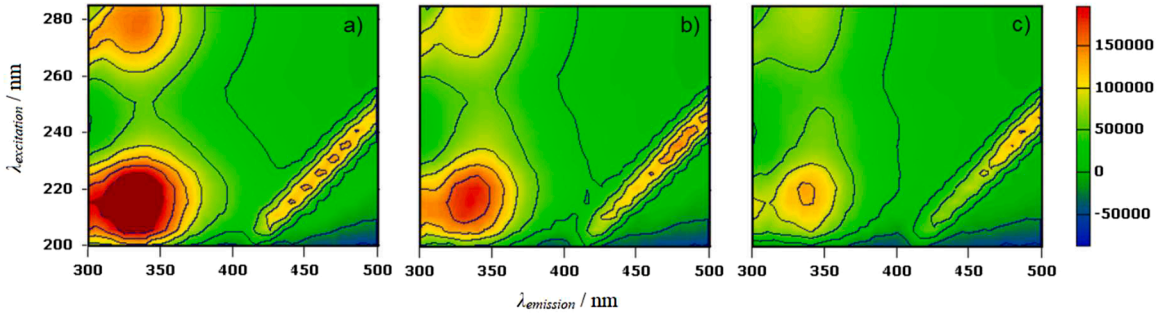

Fig. 8. Three-dimensional emission spectra of SARS-CoV-2 spike protein in absence of complex (a) and presence of an increasing concentrations of complex (**4**) ([4]/[S] = 30 (b) and [4]/[S] = 60 (c)).

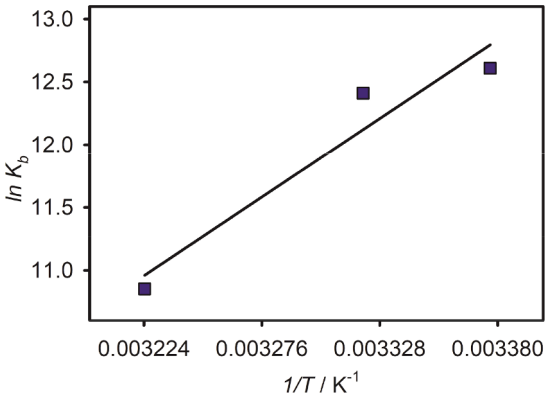

Fig. 9. van't Hoff plot for interaction of (**4**) with SARS-CoV-2 spike protein.

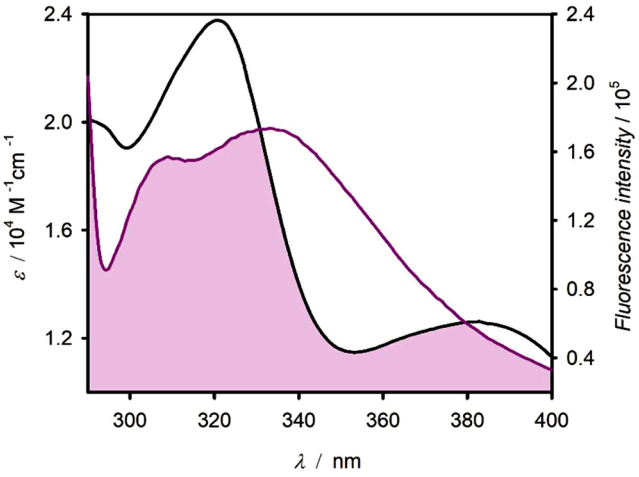

Fig. 10. The overlap of emission spectrum of SARS-CoV-2 spike protein (purple line) and absorption spectrum of (**4**) (black line).(For interpretation of the references to color in this figure legend, the reader is referred to the web version of this article.)

5-substituted derivatives with 8-hydroxyquionline (hq) coligand [47] or $[V^{V}O_2L]$ complexes of 2-acetylpyridine based hydrazones [48] and $[V^{V}O_2L]^-$ complexes of aroylhydrazonato ligands based on acid hydrazides and salicylaldehyde and 2′-hydroxyacetophenone [49] are more reactive toward DNA compared to (**1**)–(**5**) and intercalation is postulated as the most likely type of interaction.

Although the binding constants of tested oxidovanadium(IV) complexes are comparable to heteroleptic vanadium(V) complex featuring tridentate ONO donor hydrazone ligand (4,4,4-trifluoryl-1,3-

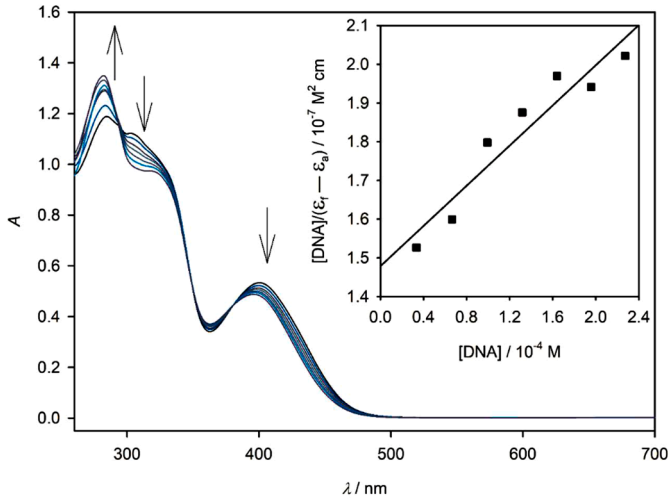

Fig. 11. Spectroscopic titration of (**1**) (5×10^{-5} M) with CT DNA in 10 mM Tris–HCl buffer pH 7.42 at 297 K. *Inset*: Graphical determination of binding constant.

Table 5
DNA binding constants of vanadium complexes (**1**)–(**5**).

Complex	K_b / M^{-1}
(**1**)	1.76×10^3
(**2**)	1.38×10^4
(**3**)	7.14×10^3
(**4**)	2.57×10^3
(**5**)	5.52×10^3

phenylbutanedione 4-chlorobenzhydrazone) and benzhydroxamic acid as a coligand the intercalation cannot be claimed as in the latter case [50]. The groove binding, as in the case of neutral oxidovanadium(V) complexes with a hydrazone scaffold containing either furan, thiophene, or pyridine residues, is to be expected [51]. This type of hydrophobic interaction is also suggested for mononuclear (alkoxido)oxidovanadium (V) with tridentate dianionic aroylazine ligands based on anthranyl- or salicylhydrazones of 2-hydroxy-1-napthaldehyde or 2-hydroxy-1-acetonaphthone [42].

To confirm the groove binding mode of oxidovanadium(IV) complexes with CT DNA the interaction of complex (**1**), having unsubstituted salicylaldehyde component of hydrazone ligand, was subjected to thermodynamic considerations. Considering that the binding constants of tested complexes with DNA vary with the change of the substituent at position 5 of the hydrazonato ligand and that the variations are within the ten-order magnitude it is reasonable to assume that the substituent

affects the binding constant, but the mode of interaction remains the same through the series of the complexes. In this contest, thermodynamics offers simple tools to gather substantial evidence on the type of binding forces that drive the interaction of small molecules with DNA. The binding constant of complex (**1**) with CT DNA was determined at three temperatures and the relevant thermodynamic data were determined from the van't Hoff plot (Table 6).

The binding constant increases with the temperature increase indicating the DNA−complex adduct is less prone to dissociation at higher temperatures and that the interactions is endothermic as obvious from the positive enthalpy change. The negative value of Gibbs free energy confirms the interaction of (**1**) with DNA is spontaneous. The positive values of enthalpy and entropy change are consistent with the hydrophobic types of the interaction and these are similar to those found for the well-known groove binder Hoechst 33,258 [52,53]. The result also further excludes intercalation, as an alternative type of hydrophobic interaction, since negative values of enthalpy and entropy changes would be anticipated [52]. Molecular docking was further employed to confirm groove binding of vanadium complexes (**1**)–(**5**) with B-DNA (PDB code: 1BNA).

The binding poses of complexes (**1**)–(**5**) to B-DNA are illustrated in Fig. 12 and total energy values for correspond interaction are summarized in Table 7. The results strongly support experimentally observed groove binding. In case of complexes (**3**) and (**5**), partial bipyridine intercalation is also anticipated by molecular docking and is in excellent agreement with experimental observed fact that these tow complexes have slightly higher values of binding constants to DNA, compared to non-substituted (**1**) and nitro-substituded (**4**) homologues (Table 5).

3.6. ADME properties of complexes

Computer-aided drug development, the estimation of absorption, distribution, metabolism and excretion (ADME) of drugs now has an important place in studies since predictive and reliable data are obtained quickly. The ADME properties of vanadium complexes were estimated using Swiss-ADME web tool. The presence of a nitro group in complex (**4**) did not allow the ADME/T property of this metal complex to be examined. The results are summarized in Supplement (Figs. S7–S10).

With the exception of complex (**3**) (532.24 g mol^{-1}), the vanadium complexes have a molecular weight less than 500 g mol^{-1}, as a key feature that determines small molecule drug homology [54], and are considered as ideal drug candidates for evaluation.

The lipophilicity properties of metal complexes encompass many parameters that play an important role in molecular exploration activities in a wide variety of fields. Lipophilicity is estimated as the consensus Log *P*, which is the mean value of all Log *P* evaluated by various lipophilicity criteria [55]. The consensus Log *P* value is highest (1.13) for (**3**) and lowest (0.25) for (**5**). The highly lipophilic nature of (**3**) appears to have greater efficacy as a transdermal drug. On the other hand, (**5**) does not show as much effect as an oral drug, as its ability to cross the cell membrane is significantly lower.

The solubility of vanadium complexes (**1**)–(**5**) is an important factor in drug-likens estimations as it provides a minimum concentration in the circulatory system, which implies better absorption in the body. SwissADME uses two methods to estimate solubility (log *S*) (topological and piecewise); where −10 and below are considered insoluble and −4 and above are considered soluble. Vanadium metal complexes appear as moderately soluble, with complex (**3**) being least soluble (log $S = -6.34$) and complex (**5**) has the highest solubility (log $S = -5.29$).

Pharmacokinetic properties of vanadium complexes, such as GI absorption, BBB permeability, PGP substrate and inhibitory activity of Cytochrome P450 isoenzymes, were also calculated. Pharmacokinetics and drug homology results indicate a high level of GI absorption for tested complexes. BBB permeant was determined as absent in all cases. However, all vanadium complexes appear to be substrates of P-gp. Complexes also appear as inhibitors of several cytochrome P450 isoenzymes.

The skin permeability coefficient (Log *K*p) is a measure of molecular penetration through the skin. The lower the Log *K*p, the less the molecule penetrates the skin [56]. Complex (**5**) is the least permeable among the complex components, while complex (**2**) is the most permeable. Compounds with high skin permeability are known to be good candidates for transdermal drugs and cosmetics rather than oral drug candidates [57].

SwissADME also provides access to five alternative rule-based filters, each with different properties, where the molecule is classified as drug-like. All tested vanadium complexes have good Druglikness properties, except complex (**2**) and (**3**) where "No" is found for Ghose (Amgen) parameter. The obtained results candidate reported vanadium complexes as potential drugs which are suitable for further biological evaluation.

Table 6
Thermodynamic data on DNA – complex (**1**) interaction.

t /°C	K_b / M^{-1}	ln *K*	Δ*H* / kJ mol^{-1}	Δ*S* / J mol^{-1} K^{-1}	Δ*G* / kJ mol^{-1}
18	1.12×10^3	7.021	71	300	−16.9
24	1.76×10^3	7.473			−18.7
30	3.55×10^3	8.175			−20.5

3.7. Antioxidant activity

The antioxidant activity of vanadium complexes is not thoroughly documented in the literature and is inevitably investigated when ligand-based antioxidant activity is expected, as in the case of vanadium flavonoid complexes [58,59]. The antioxidant activity of free ligands is regularly lower compared to corresponding vanadium complexes, as generally observed for many metal complexes [60–62]. As the antioxidant activity plays a major role in drug discovery vanadium complexes (**1**)–(**5**) were screened for their radical scavenging activity. The antioxidant of oxidovanadium(IV) hydrazone complexes (**1**)–(**5**) is anticipated based on its V(IV) oxidation state and the fact that the substitution of organic molecules greatly affects their antioxidant potential [63,64]. The DPPH radical scavenging ability of complexes is presented in Table 8. The strongest antioxidant activity was found for complex (**5**) featuring 5-hydroxy substituent on the salicylaldehyde component of furoic acid hydrazone. This remarkably low IC_{50} value for complex (**5**) is comparable to ascorbic acid. Very promising antioxidant activity was also observed for complex (**4**) with a nitro substituent. Nitro groups are documented to increase antioxidant activity [65]. The IC_{50} values for complexes (**1**)–(**4**) can be correlated to corresponding half-wave potentials for V^V/V^{IV} couple that we reported earlier [15]. As the half-wave potential of the V^V/V^{IV} couple becomes more positive the IC_{50} value lowers. This indicates the antioxidant mechanism by which vanadium complexes (**1**)–(**4**) show their antioxidant activity include single electron transfer (SET). However, complex (**5**) deviates from this behavior since it has ionisable phenolic group on hydrazone ligand and additionally can show antioxidant activity by hydrogen atom transfer (HAT) mechanism.

4. Conclusion

In the past two years, several studies based on molecular docking nominated vanadium compounds as druggable toward proteins of SARS-CoV-2 virus. Given that in the field of medicinal chemistry, the design and development of new antiviral drugs is of key importance due to the specificities associated with the life cycle of viruses compared to well-known targets on bacteria or tumors, we aimed to test this hypothesis under experimental conditions. Oxidovanadium(IV) complexes

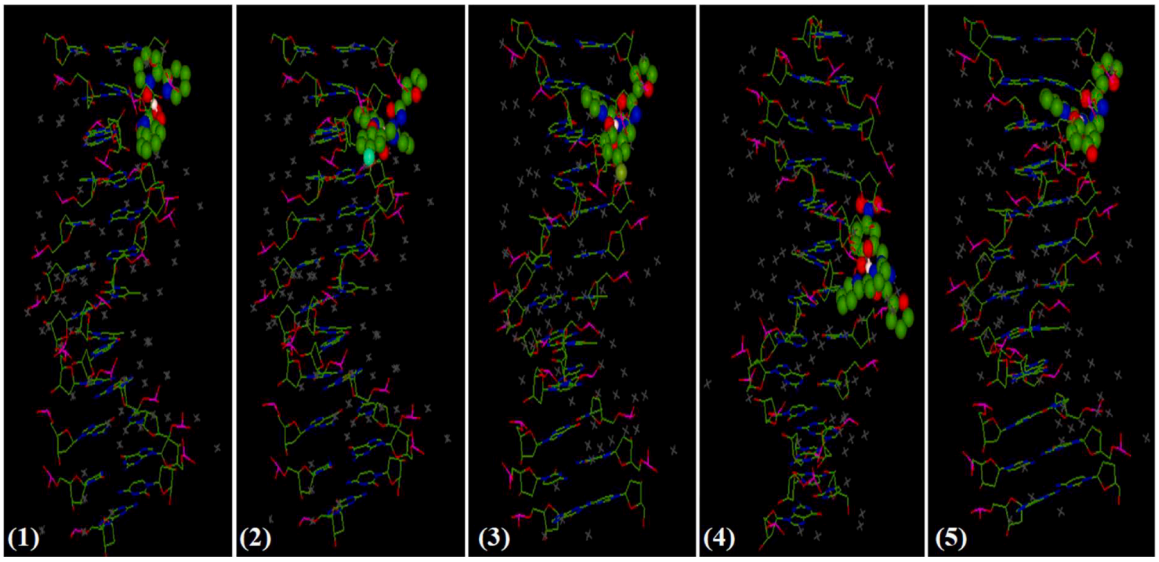

Fig. 12. Binding poses of (**1**)–(**5**) complexes to B-DNA.

Table 7
The total energy values (kcal/mol) for the interaction of (**1**)–(**5**) with B-DNA.

	E_{total}
(**1**)	−299.79
(**2**)	−289.96
(**3**)	−304.10
(**4**)	−296.91
(**5**)	−293.56

Table 8
Antioxidant activity of vanadium complexes (**1**)–(**5**).

Sample	IC_{50} / μM
(**1**)	77 ± 7
(**2**)	34 ± 1
(**3**)	37 ± 2
(**4**)	24 ± 1
(**5**)	21 ± 2
Ascorbic acid	24 ± 2

featuring hydrazone ligands derived from salicylaldehyde and 2-furoic acid hydrazide reported earlier by our group were selected for testing as weakly albumin-reactive species and were subjected to molecular docking to assess their potential to bind SARS-CoV-2 spike protein. The theoretical predictions indicate that complexes are reactive to spike protein and that the reactivity is affected by the electronic effects caused by the substituent on the salicylaldehyde component of the hydrazone ligand. The electron-withdrawing nitro group has a significant effect in binding the complex to spike protein. The complex binds predominantly to the spike protein through van der Walls interactions and hydrogen bonding. The very high binding constant, 30 times higher compared to the binding constant of the complex to albumin, candidate these complexes as potential anti-SARS-CoV-2 agents targeting spike protein and distinguish them from majority of generally albumin-reactive vanadium complexes. FRET analysis suggested a static fluorescence quenching mechanism and non-radiative energy transfer. Complexes demonstrated ability to interact with SARS-CoV-2 omicron variant (BA.1) RBD with human ACE2 protein in silico and more pronounced hydrophobic interactions, as well as hydrogen bonding, were observed compared to SARS-CoV-2 spike protein. However, in case of both proteins, interaction of complexes with amino acid residues were not close to spike protein – ACE2 interface. Also, the complexes showed a moderate affinity towards DNA, as a potential intracellular target of new drugs, and moderate K_b values, coupled with positive ΔH and ΔS values indicate groove binding. Groove binding was confirmed by molecular docking with B-DNA. Complexes possess good druglikness properties as assessed by SwissADME analysis and strong antioxidant activity in vitro. These results nominate oxidovanadium(IV) hydrazone complexes as target-selective and spike protein-reactive agents in vitro. The results presented are not an end in themselves and for the first time experimentally confirm that vanadium compounds could be druggable against SARS-CoV-2 even more than it is predicted by molecular docking thus giving an evidence-based rationale for the design and development of new vanadium compounds as selective and reactive antiviral agents.

Funding

This work was supported by the Ministry of Science, Higher Education and Youth of the Canton of Sarajevo under grant no. 27-02-11-41251-2/21 (Adnan Zahirović).

Supplementary materials

Supplementary material associated with this article can be found in the online version.

CRediT authorship contribution statement

Adnan Zahirović: Conceptualization, Formal analysis, Funding acquisition, Investigation, Methodology, Visualization, Supervision, Writing – original draft, Writing – review & editing. **Burak Tüzün:** Methodology, Software, Writing – original draft. **Selma Hadžalić:** Formal analysis, Investigation, Visualization. **Irnesa Osmanković:** Investigation. **Sunčica Roca:** Investigation, Writing – original draft. **Sabina Begić:** Investigation. **Muhamed Fočak:** Conceptualization, Writing – original draft, Writing – review & editing.

Declaration of Competing Interest

The authors declare that they have no known competing financial interests or personal relationships that could have appeared to influence the work reported in this paper.

Data availability

Data will be made available on request.

Acknowledgments

The numerical calculations reported in this paper were fully/partially performed at TUBITAK ULAKBIM, High Performance and Grid Computing Center (TRUBA resources).

Supplementary materials

Supplementary material associated with this article can be found, in the online version, at doi:10.1016/j.molstruc.2023.136564.

References

[1] C. Zhang, Y. Li, J. Cao, X. Wen, On the mass COVID-19 vaccination scheduling problem, Comput. Oper. Res. 141 (2022), 105704.
[2] E.A. Harrison, J.W. Wu, Vaccine confidence in the time of COVID-19, Eur. J. Epidemiol. 35 (4) (2020) 325–330.
[3] J.A. Malik, S. Ahmed, A. Mir, M. Shinde, O. Bender, F. Alshammari, M. Ansari, S. Anwar, The SARS-CoV-2 mutation versus vaccine effectiveness: new opportunities to new challenges, J.Infect. Public Health 15 (2) (2022) 228–240.
[4] L. Dong, S. Hu, J. Gao, Discovering drugs to treat coronavirus disease 2019 (COVID-19), Drug Discov. Ther. 14 (1) (2020) 58–60.
[5] T. Scior, H.H. Abdallah, S.F.Z. Mustafa, J.A. Guevara-García, D. Rehder, Are vanadium complexes druggable against the main protease M^{pro} of SARS-CoV-2?—A computational approach, Inorg. Chim. Acta 519 (2021), 120287.
[6] M.C. Vlasiou, K.S. Pafti, Screening possible drug molecules for COVID-19. The example of vanadium (III/IV/V) complex molecules with computational chemistry and molecular docking, Comput. Toxicol. 18 (2021), 100157.
[7] Ł. Popiołek, Hydrazide–hydrazones as potential antimicrobial agents: overview of the literature since 2010, Med. Chem. Res. 26 (2) (2017) 287–301.
[8] S. Rollas, Ş.G. Küçükgüzel, Biological activities of hydrazone derivatives, Molecules 12 (8) (2007) 1910–1939.
[9] O.J. D'Cruz, Y. Dong, F.M. Uckun, Potent dual anti-HIV and spermicidal activities of novel oxovanadium(V) complexes with thiourea non-nucleoside inhibitors of HIV-1 reverse transcriptase, Biochem. Biophys. Res. Commun. 302 (2) (2003) 253–264.
[10] S.-Y. Wong, R.W.-Y. Sun, N.P.-Y. Chung, C.-L. Lin, C.-M. Che, Physiologically stable vanadium (IV) porphyrins as a new class of anti-HIV agents, Chem. Commun. (28) (2005) 3544–3546.
[11] S. Shigeta, S. Mori, E. Kodama, J. Kodama, K. Takahashi, T. Yamase, Broad spectrum anti-RNA virus activities of titanium and vanadium substituted polyoxotungstates, Antivir. Res. 58 (3) (2003) 265–271.
[12] D. Rogolino, M. Carcelli, A. Bacchi, C. Compari, L. Contardi, E. Fisicaro, A. Gatti, M. Sechi, A. Stevaert, L. Naesens, A versatile salicyl hydrazonic ligand and its metal complexes as antiviral agents, J. Inorg. Biochem. 150 (2015) 9–17.
[13] E. Lukevits, L. Demicheva, Biological activity of furan derivatives, Chem. Heterocycl. Compd. 29 (3) (1993) 243–267.
[14] R. Banerjee, H. Kumar, M. Banerjee, Medicinal significance of furan derivatives: a review, Int. J. Res. Phytochem. Pharmacol. 5 (3) (2015) 48–57.
[15] A. Zahirović, S. Hadžalić, A. Višnjevac, M. Fočak, B. Tüzün, D. Žilić, S. Roca, J. Jurec, A. Topčagić, I. Osmanković, Vanadium (IV) complexes of salicylaldehyde-based furoic acid hydrazones: synthesis, BSA binding and in vivo antidiabetic potential, J. Inorg. Biochem. 244 (2023), 112232.
[16] C.B. Jackson, M. Farzan, B. Chen, H. Choe, Mechanisms of SARS-CoV-2 entry into cells, Nat. Rev. Mol. Cell Biol. 23 (1) (2022) 3–20.
[17] W. Su, S.F. Sia, A.J. Schmitz, T.L. Bricker, T.N. Starr, A.J. Greaney, J.S. Turner, B. M. Mohammed, Z. Liu, K.T. Choy, Neutralizing monoclonal antibodies that target the spike receptor binding domain confer Fc receptor-independent protection against SARS-CoV-2 infection in Syrian hamsters, mBio 12 (5) (2021) 1–16, e0239521.
[18] A. Zahirović, S. Roca, E. Kahrović, A. Višnjevac, Low DNA and high BSA binding affinity of cationic ruthenium (II) organometallic featuring pyridine and 2′-hydroxychalcone ligands, J. Mol. Struct. 1236 (2021), 130326.
[19] K.G. Gurevich, Effect of blood protein concentrations on drug-dosing regimes: practical guidance, Theor. Biol. Med. Model. 10 (1) (2013) 1–7.
[20] R.T. Scheife, Protein binding: what does it mean? Dicp 23 (7-8) (1989) S27–S31.
[21] M. Liu, Z.J. Lim, Y.Y. Gwee, A. Levina, P.A. Lay, Characterization of a ruthenium (III)/NAMI-A adduct with bovine serum albumin that exhibits a high anti-metastatic activity, Angew. Chem. 122 (9) (2010) 1705–1708.
[22] V.K. Garg, H. Avashthi, A. Tiwari, P.A. Jain, P.W. Ramkete, A.M. Kayastha, V. K. Singh, MFPPI–multi FASTA ProtParam interface, Bioinformation 12 (2) (2016) 74.
[23] W. Brand-Williams, M.-E. Cuvelier, C. Berset, Use of a free radical method to evaluate antioxidant activity, LWT-Food Sci. Technol. 28 (1) (1995) 25–30.
[24] D. Ritchie, T. Orpailleur, Hex 8.0. 0 User Manual, Protein Docking Using Spherical Polar Fourier Correlations Copyright c (2013).
[25] M.F. Adasme, K.L. Linnemann, S.N. Bolz, F. Kaiser, S. Salentin, V.J. Haupt, M. Schroeder, PLIP 2021: expanding the scope of the protein–ligand interaction profiler to DNA and RNA, Nucl. Acids Res. 49 (W1) (2021) W530–W534.
[26] C. Zhang, Y. Wang, Y. Zhu, C. Liu, C. Gu, S. Xu, Y. Wang, Y. Zhou, Y. Wang, W. Han, Development and structural basis of a two-MAb cocktail for treating SARS-CoV-2 infections, Nat. Commun. 12 (1) (2021) 264.
[27] Q. Geng, K. Shi, G. Ye, W. Zhang, H. Aihara, F. Li, Structural basis for human receptor recognition by SARS-CoV-2 Omicron variant BA. 1, J. Virol. 96 (8) (2022) 1–9, e00249-22.
[28] H.R. Drew, R.M. Wing, T. Takano, C. Broka, S. Tanaka, K. Itakura, R.E. Dickerson, Structure of a B-DNA dodecamer: conformation and dynamics, Proc. Natl. Acad. Sci. 78 (4) (1981) 2179–2183.
[29] D. Favre, J.F. Harmon, A. Zhang, M.S. Miller, I.A. Kaltashov, Decavanadate interactions with the elements of the SARS-CoV-2 spike protein highlight the potential role of electrostatics in disrupting the infectivity cycle, J. Inorg. Biochem. 234 (2022), 111899.
[30] X. Xia, Domains and functions of spike protein in Sars-Cov-2 in the context of vaccine design, Viruses 13 (1) (2021) 109.
[31] D. Majumdar, J.E. Philip, B. Tüzün, A. Frontera, R.M. Gomila, S. Roy, K. Bankura, Unravelling the synthetic mimic, spectroscopic insights, and supramolecular crystal engineering of an innovative heteronuclear Pb (II)-salen cocrystal: an integrated DFT, QTAIM/NCI plot, NLO, molecular docking/PLIP, and antibacterial appraisal, J. Inorg. Organomet. Polym. Mater. 32 (11) (2022) 4320–4339.
[32] M. Tapera, H. Kekeçmuhammed, B. Tüzün, E. Sarıpınar, Ü.M. Koçyiğit, E. Yıldırım, M. Doğan, Y. Zorlu, Synthesis, carbonic anhydrase inhibitory activity, anticancer activity and molecular docking studies of new imidazolyl hydrazone derivatives, J. Mol. Struct. 1269 (2022), 133816.
[33] D. İnci, R. Aydın, Ö. Vatan, T. Sevgi, D. Yılmaz, Y. Zorlu, Y. Yerli, B. Çoşut, E. Demirkan, N. Çinkılıç, Synthesis and crystal structures of novel copper (II) complexes with glycine and substituted phenanthrolines: reactivity towards DNA/BSA and in vitro cytotoxic and antimicrobial evaluation, JBIC J. Biol. Inorg. Chem. 22 (2017) 61–85.
[34] U.K. Aravind, J. Mathew, C. Aravindakumar, Transport studies of BSA, lysozyme and ovalbumin through chitosan/polystyrene sulfonate multilayer membrane, J. Memb. Sci. 299 (1-2) (2007) 146–155.
[35] P.D. Ross, S. Subramanian, Thermodynamics of protein association reactions: forces contributing to stability, Biochemistry 20 (11) (1981) 3096–3102.
[36] A. Zahirović, D. Žilić, S.K. Pavelić, M. Hukić, S. Muratović, A. Harej, E. Kahrović, Type of complex–BSA binding forces affected by different coordination modes of alliin in novel water-soluble ruthenium complexes, New J. Chem. 43 (15) (2019) 5791–5804.
[37] A. Zahirović, I. Osmanković, A. Osmanović, A. Višnjevac, A. Magoda, S. Hadžalić, E. Kahrović, Interaction of copper (II) complexes of bidentate benzaldehyde nicotinic acid hydrazones with BSA: spectrofluorimetric and molecular docking approach, Acta Chim. Slov. 70 (1) (2023) 74–85.
[38] F. Wang, W. Huang, Z. Dai, Spectroscopic investigation of the interaction between riboflavin and bovine serum albumin, J. Mol. Struct. 875 (1-3) (2008) 509–514.
[39] P. Naik, S. Chimatadar, S. Nandibewoor, Study on the interaction between antibacterial drug and bovine serum albumin: A spectroscopic approach, Spectrochim. Acta Part A 73 (5) (2009) 841–845.
[40] D. İnci, R. Aydın, Ö. Vatan, T. Sevgi, D. Yılmaz, Y. Zorlu, Y. Yerli, B. Çoşut, E. Demirkan, N. Çinkılıç, Synthesis and crystal structures of novel copper (II) complexes with glycine and substituted phenanthrolines: reactivity towards DNA/BSA and in vitro cytotoxic and antimicrobial evaluation, JBIC J. Biol. Inorg. Chem. 22 (1) (2017) 61–85.
[41] S.K. Nandanwar, H.J. Kim, Anticancer and antibacterial activity of transition metal complexes, ChemistrySelect 4 (5) (2019) 1706–1721.
[42] S.P. Dash, A.K. Panda, S. Dhaka, S. Pasayat, A. Biswas, M.R. Maurya, P.K. Majhi, A. Crochet, R. Dinda, A study of DNA/BSA interaction and catalytic potential of oxidovanadium (V) complexes with ONO donor ligands, Dalton Trans. 45 (45) (2016) 18292–18307.
[43] E. Kahrović, A. Zahirović, E. Turkušić, S. Bektaš, A dinuclear ruthenium (II) Schiff base complex with dissimilar coordination: synthesis, characterization, and biological Activity, Z. Anorg. Allg. Chem. 642 (6) (2016) 480–485.
[44] S. Kothandan, A. Sheela, DNA interaction and cytotoxic studies on mono/di-oxo and peroxo-vanadium (V)complexes—A review, Mini Rev. Med. Chem. 21 (14) (2021) 1909–1924.
[45] M.S.S. Adam, O.M. El-Hady, M.M. Makhlouf, A. Bayazeed, N.M. El-Metwaly, A.D. M. Mohamad, Effect of oxy-vanadium (IV) and oxy-zirconium (IV) ions in O, *N*-bidentate arylhydrazone complexes on their catalytic and biological potentials that supported via computerized usages, J. Taiwan Inst. Chem. Eng. 132 (2022), 104168.
[46] S.A. Aboafia, S.A. Elsayed, A.K. El-Sayed, A.M. El-Hendawy, New transition metal complexes of 2, 4-dihydroxybenzaldehyde benzoylhydrazone Schiff base (H2dhbh): synthesis, spectroscopic characterization, DNA binding/cleavage and antioxidant activity, J. Mol. Struct. 1158 (2018) 39–50.
[47] W. Jing-lin, Z. Ya-qin, Y. Bin-sheng, Transition metal complexes of asymmetrical aroyl-hydrazone ligand: syntheses, structures, DNA binding and cleavage studies, Inorg. Chim. Acta 409 (2014) 484–496.
[48] S.P. Dash, A.K. Panda, S. Pasayat, S. Majumder, A. Biswas, W. Kaminsky, S. Mukhopadhyay, S.K. Bhutia, R. Dinda, Evaluation of the cell cytotoxicity and DNA/BSA binding and cleavage activity of some dioxidovanadium(V) complexes containing aroylhydrazones, J. Inorg. Biochem. 144 (2015) 1–12.
[49] S.P. Dash, A.K. Panda, S. Pasayat, R. Dinda, A. Biswas, E.R. Tiekink, Y.P. Patil, M. Nethaji, W. Kaminsky, S. Mukhopadhyay, Syntheses and structural investigation of some alkali metal ion-mediated $LV^{V}O_2^-$ (L^{2-} = tridentate ONO

ligands) species: DNA binding, photo-induced DNA cleavage and cytotoxic activities, Dalton Trans. 43 (26) (2014) 10139–10156.
[50] P. Inamdar, S. Angappan, DNA binding behaviour of mixed ligand vanadium(V) complex based on novel tridentate hydrazone and benzhydroxamic acid ligand systems, Appl. Organomet. Chem. 31 (3) (2017) e3573.
[51] S.P. Dash, A.K. Panda, S. Pasayat, R. Dinda, A. Biswas, E.R. Tiekink, S. Mukhopadhyay, S.K. Bhutia, W. Kaminsky, E. Sinn, Oxidovanadium(V) complexes of Aroylhydrazones incorporating heterocycles: synthesis, characterization and study of DNA binding, photo-induced DNA cleavage and cytotoxic activities, RSC Adv. 5 (64) (2015) 51852–51867.
[52] J.B. Chaires, Energetics of drug–DNA interactions, Biopolymers 44 (3) (1997) 201–215.
[53] I. Haq, Thermodynamics of drug–DNA interactions, Arch. Biochem. Biophys. 403 (1) (2002) 1–15.
[54] A. Daina, O. Michielin, V. Zoete, SwissADME: a free web tool to evaluate pharmacokinetics, drug-likeness and medicinal chemistry friendliness of small molecules, Sci. Rep. 7 (1) (2017) 42717.
[55] D. Ranjith, C. Ravikumar, SwissADME predictions of pharmacokinetics and drug-likeness properties of small molecules present in *Ipomoea mauritiana* Jacq, J. Pharmacogn. Phytochem. 8 (5) (2019) 2063–2073.
[56] M.A. Maciel Tabosa, M. Hoppel, A.L. Bunge, R.H. Guy, M.B. Delgado-Charro, Predicting topical drug clearance from the skin, Drug Deliv. Transl. Res. 11 (2021) 729–740.
[57] R.O. Potts, R.H. Guy, Predicting skin permeability, Pharm. Res. 9 (1992) 663–669.
[58] S. Roy, S. Mallick, T. Chakraborty, N. Ghosh, A.K. Singh, S. Manna, S. Majumdar, Synthesis, characterisation and antioxidant activity of luteolin–vanadium (II) complex, Food Chem. 173 (2015) 1172–1178.
[59] S. Roy, S. Majumdar, A.K. Singh, B. Ghosh, N. Ghosh, S. Manna, T. Chakraborty, S. Mallick, Synthesis, characterization, antioxidant status, and toxicity study of vanadium–rutin complex in Balb/c mice, Biol. Trace Elem. Res. 166 (2) (2015) 183–200.
[60] R.C. Marchi, I.A. Campos, V.T. Santana, R.M. Carlos, Chemical implications and considerations on techniques used to assess the in vitro antioxidant activity of coordination compounds, Coord. Chem. Rev. 451 (2022), 214275.
[61] E. Rodríguez-Arce, M. Saldías, Antioxidant properties of flavonoid metal complexes and their potential inclusion in the development of novel strategies for the treatment against neurodegenerative diseases, Biomed. Pharmacother. 143 (2021), 112236.
[62] A. Zahirović, E. Kahrović, M. Cindrić, S. Kraljević Pavelić, M. Hukić, A. Harej, E. Turkušić, Heteroleptic ruthenium bioflavonoid complexes: from synthesis to in vitro biological activity, J. Coord. Chem. 70 (24) (2017) 4030–4053.
[63] M. Plaza, T. Pozzo, J. Liu, K.Z. Gulshan Ara, C. Turner, E. Nordberg Karlsson, Substituent effects on in vitro antioxidizing properties, stability, and solubility in flavonoids, J. Agric. Food Chem. 62 (15) (2014) 3321–3333.
[64] H.S. Kareem, A. Ariffin, N. Nordin, T. Heidelberg, A. Abdul-Aziz, K.W. Kong, W. A. Yehye, Correlation of antioxidant activities with theoretical studies for new hydrazone compounds bearing a 3, 4, 5-trimethoxy benzyl moiety, Eur. J. Med. Chem. 103 (2015) 497–505.
[65] H. Randhawa, A. Kamboj, A.K. Saluja, Synthesis, pharmacological evaluation and computational studies of some novel hydrazine derivatives of thiophene chalcone as antimicrobial and antioxidant agents, World J. Pharm. Res. 3 (2014) 3146–3159.